Macromolecules

pubs.acs.org/Macromolecules
Article

Comparison of the Swelling Behavior of Poly(*N*-Isopropylacrylamide) and Poly(*N*-Vinylisobutyramide) Thin Films under Water Vapor Exposure

Morgan P. Le Dû, Julija Reitenbach, David P. Kosbahn, Lukas V. Spanier, Robert Cubitt, Cristiane Henschel, André Laschewsky, Christine M. Papadakis, and Peter Müller-Buschbaum*

Cite This: *Macromolecules* 2025, 58, 1000−1010

ABSTRACT: Poly(*N*-isopropylacrylamide) (PNIPAM) is known for exhibiting lower critical solution temperature behavior in water. A structural isomer of PNIPAM, the likewise LCST-type polymer poly(*N*-vinylisobutyramide) (PNVIBAM), is compared to PNIPAM in a thin film with respect to their swelling behaviors and water uptake kinetics in a humid atmosphere. Based on spectral reflectance, Fourier-transform infrared (FT-IR) spectroscopy, and time-of-flight neutron reflectometry, the amount and kinetics of uptaken water and its distribution inside the films correlate with molecular changes. It is observed that PNVIBAM swells less than PNIPAM. The FT-IR signals reveal a lower water affinity for PNVIBAM than for PNIPAM and larger hydrophobic clathrates in PNVIBAM, which hinders the introduction of water. Additionally, N_2-dried PNIPAM films still contain primary water, whereas PNVIBAM can be fully dried. The first step of water uptake of the main layer describes a filling of the free volume, reaching a water content of 3.8% in PNVIBAM and 6% in PNIPAM.

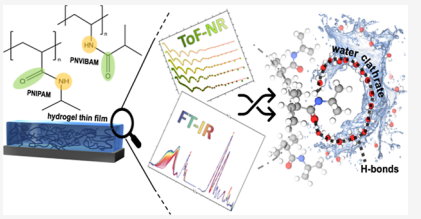

INTRODUCTION

Stimuli-responsive polymers represent a diverse class of polymers with great potential, as these polymers exhibit the remarkable ability to respond strongly to external stimuli.[1−5] They undergo conformational changes triggered by external factors, including alterations in pH,[6] exposure to light,[7] application of electric fields,[8] changes in temperature[9] and in pressure,[10] or chemical modifications of the surrounding environment.[11−13] In particular, when applied as thin films, the intrinsic responsiveness enables stimuli-responsive polymers to serve as versatile building blocks in fields ranging from drug delivery systems and biosensors[14−17] to actuators[18] and responsive coatings.[19] Among them, thermoresponsive polymers offer extensive options as the temperature stimulus is easily accessible and noninvasive. Such polymers undergo a conformational change and a change of solvation state in response to temperature variation with two possible scenarios.[20] On the one hand, lower critical solution temperature (LCST)-type polymers can be identified as becoming insoluble upon heating. On the other hand, upper critical solution temperature-type polymers become soluble with increasing temperature.[9,21] Both types of thermoresponsive polymers can be engineered to adopt hydrogel states, wherein entangled polymer chains create a hydrophilic three-dimensional network through physical or chemical cross-links.[22,23] Hydrogels are characterized by their ability to retain water molecules within their matrix while maintaining a soft solid-like morphology.[13,24−28] Combining the thermal response with their water absorption capacity, thermoresponsive hydrogels are the perfect candidates for a controlled drug delivery system.[15] With an increase in temperature, they can release the desired small molecules formerly incorporated within their matrix.

Poly(*N*-isopropylacrylamide) (PNIPAM) is one of the most outstanding thermoresponsive polymers and has been studied for its sharp and reversible phase transition at around 30 °C in aqueous solutions.[29,30] The conformational change experienced by PNIPAM is commonly described as a "coil-to-globule" transition. This transition involves a change from the coil-like and expanded shape of the polymer chains below the phase transition temperature, which facilitates the polymer's hydration, to a globular "collapsed" morphology where most water molecules are expelled from the polymer's solvation shell. This behavior of PNIPAM arises from the delicate balance between its hydrophobic moieties, such as the isopropyl group, methylene groups of the polymer backbone, and the amide group acting as a hydrophilic unit.[12,31,32]

The large number of fundamental studies makes PNIPAM a well-developed model polymer. However, the acrylamide-based monomers used for the synthesis of NIPAM-based polymers pose toxicity risks,[33] and their intensive use has

Received: November 13, 2024
Revised: December 16, 2024
Accepted: December 23, 2024
Published: January 6, 2025

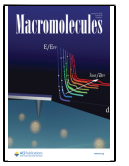

https://doi.org/10.1021/acs.macromol.4c02802
Macromolecules 2025, 58, 1000−1010

brought substantial traces of acrylamides in food and water wastes.[34−36] Hence, PNIPAM alternatives are under investigation, such as *N*-vinylalkylamide-based monomers, which are conformational isomers of their *N*-alkylacrylamide analogues, and appear to be a suitable alternative due to their good biological compatibility.[37−39] In particular, poly(*N*-vinylisobutyramide) (PNVIBAM) is selected for investigation in this study as an isomer of PNIPAM (Figure 1),[10,40−44]

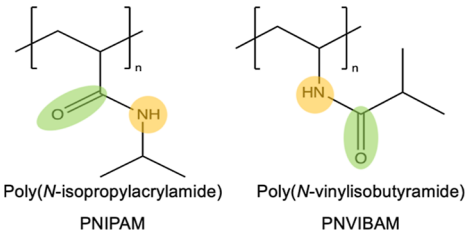

Figure 1. Chemical structures of the structural isomers ($C_6H_{11}NO$) PNIPAM (left) and PNVIBAM (right) with the amide functional groups and their relative positions to the polymer backbones highlighted.

wherein the amide linkage relative to the polymer backbone is reversed. Specifically, in the case of PNVIBAM, the amide's −NH group is linked to the polymer backbone, whereas in PNIPAM, the carbonyl −C═O group is attached to the backbone. Similar to PNIPAM, PNVIBAM is also water-soluble and features LCST-type II behavior,[41,45] while other structural isomers of PNIPAM (chemical formula $(C_6H_{11}NO)_n$) also containing secondary amide groups, such as poly(leucine) or poly(caprolactam) (nylon-6), are completely water-insoluble. Notably, PNVIBAM undergoes a coil-to-globule transition at approximately 39 °C in water.[41,46,47] This characteristic renders PNVIBAM particularly appealing for medical applications, as its transition temperature is closer to the human body temperature (ca. 37 °C) compared to the LCST of PNIPAM of about 30 °C.[48] Furthermore, the LCST of PNVIBAM falls within the range of an elevated body temperature, making it an even more attractive option for controlled drug delivery and smart coating applications, e.g., in the case of infections or inflammations where PNVIBAM micelles or/and skin-coating can collapse and release desired medicine when the body temperature reaches the polymer's phase transition temperature. Yet, PNVIBAM has received significantly less attention than PNIPAM.

The present study focuses on PNVIBAM thin films, which have been virtually unexplored.[40] In the thin film geometry, the inherent high polymer concentration, the two-dimensional confinement of the polymer chains within the film structure, as well as the presence of interfaces with the substrate and the surrounding atmosphere impose additional differences from studies of classical volume samples. We compare the swelling behavior of PNVIBAM thin films in a water vapor atmosphere with that of PNIPAM thin films, which have already been studied before.[49,50] We investigate the solvation process of PNVIBAM and compare it to the one of the well-known PNIPAM at multiple levels ranging from mesoscopic to molecular scale. Spectral reflectance (SR) is used to examine the in situ thickness evolution of the films over time under humid conditions at the mesoscopic level. At the molecular level, the solvation of the films is explored using in situ Fourier-transform infrared (FT-IR) spectroscopy to understand the hydration mechanisms of PNVIBAM in relation to its isomer PNIPAM. Relevant information about thin film geometry is gained with time-of-flight neutron reflectometry (ToF-NR), enabling an in-depth description of the inner structure of these films without damaging the samples. In addition, neutron characterizations offer an enhanced contrast when heavy water is used (D_2O). This approach enables the study of the evolution of the solvent distribution within the films during the swelling process.

EXPERIMENTAL SECTION

Materials and Sample Preparation. *Materials.* Silicon wafers (p/Bor, <100>, d = 525 ± 25 μm, 10−20 Ω × cm) from Si-Mat, Kaufering, Germany, were used as substrates for the film preparation. For the acid bath cleaning of the substrates, we used deionized water, sulfuric acid (H_2SO_4, 95−98%, Aldrich), and hydrogen peroxide (H_2O_2, 30% aq., Roth) as received. All of the water used in this study was deionized to a resistivity of 18.2 MΩ × cm using a Milli-Q Plus purification system (Merck Millipore, Burlington, U.S.A.). PNIPAM solutions were prepared from poly(*N*-isopropylacrylamide) from Sigma-Aldrich (PNIPAM, $M_n \approx 40$ kg/mol, T_{mp} = 96 °C) and stored in the dark at 4 °C. PNVIBAM solutions were prepared from PNVIBAM synthesized by free radical polymerization, resulting in a number-average molar mass of M_n = 43 kg/mol (more details can be found in the Supporting Information). The number-average molar mass of both isomers is considered to be similar and, therefore, suitable for this comparative study. 1,4-dioxane (≥99.5%, Aldrich) was used as received as a solvent for the polymer solutions. Deionized light water (DI H_2O) was utilized for vapor exposure. In the case of vapor exposure during ToF-NR characterization, heavy water (D_2O, 99.95%, Deutero GmbH) was used.

Sample Preparation for SR and ToF-NR. Solutions of the PNIPAM and PNVIBAM homopolymers were prepared in 1,4-dioxane at various concentrations (Supporting Information). The polymer solutions were placed on a lab shaker for 24 h to ensure homogenized dissolution. Next, the solutions were filtered through hydrophobic polytetrafluoroethylene membrane filters (0.45 μm pore size, Merck Millipore, Burlington, U.S.A.) to remove insoluble impurities. Precut silicon wafers were submerged in an acid bath (54 mL DI water, 84 mL H_2O_2, and 198 mL H_2SO_4) at 80 °C for 30 min, carefully rinsed with DI water, dried using N_2, and treated with oxygen plasma (240 W) at 0.4 mbar for 20 min. Immediately afterward, thin polymer films were deposited via spin-coating (2500 rpm, 60 s, V = 0.2 mL for SR samples, and V = 3.0 mL for ToF-NR samples). The obtained samples were stored in a desiccator.

Sample Preparation for FT-IR Spectroscopy. The polymer solutions of PNIPAM and PNVIBAM homopolymers in 1,4-dioxane were prepared with a concentration of 14 mg/mL. The precut silicon substrates were treated with oxygen plasma (240 W) at 0.4 mbar for 20 min. Next, 70.0 μL of the polymer solution was drop-cast onto a substrate. After being dried for 1 h, the resulting samples were placed in a custom-made copper sample cell for FT-IR characterization.

METHODS

Spectral Reflectance Measurements. SR measurements were performed using a custom-made sample environment described in the Supporting Information and a Filmetrics F20 Thin-Film Analyzer (KLA, Milpitas, U.S.A.) with a halogen lamp light source (λ = 380−1100 nm) and a spectrometer.

In Situ Fourier-Transform Infrared Spectroscopy. FT-IR spectra were collected by using an Equinox 55 FT-IR spectrometer (Bruker Optik GmbH, Rosenheim, Germany). A detailed description is provided in the Supporting Information. The temperature of the sample environment was precisely controlled by using a circulating thermal bath and maintained at 19 °C throughout the experiment. First, the samples underwent a drying process under N_2 for a duration of 1 h, following which an initial spectrum was recorded. Subsequently, the humidity conditions were established by switching off the N_2 flow, and the water vapors were introduced into the sample

https://doi.org/10.1021/acs.macromol.4c02802
Macromolecules 2025, 58, 1000−1010

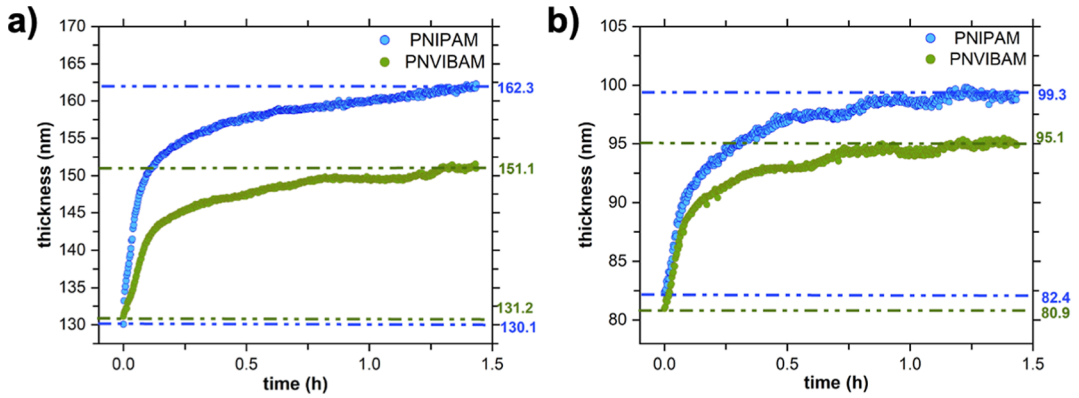

Figure 2. Thickness evolution over time of PNIPAM and PNVIBAM films recorded by SR for films with an initial thickness of (a) ∼130 nm and (b) ∼81 nm.

environment through a connecting hole (approximately 1 mm in diameter), leading to the reservoir containing 0.4 mL of DI water.

Time-of-Flight Neutron Reflectometry. The ToF-NR measurements were carried out at instrument D17 at the Institut Laue-Langevin (ILL) site in Grenoble, France.[51,52] More details about the measurement settings and the data analysis can be found in the Supporting Information. The scattering length densities (SLD) for both isomers were calculated and found to be about 0.810×10^{-6} Å^{-2}. The SLD values of the substrate were maintained at constant values of 2.065×10^{-6} Å^{-2} for the Si substrate and 3.25×10^{-6} Å^{-2} for the SiO_x native oxide layer on the surface of the substrate.[12] Regarding the SLD of the solvents involved during the experiments, the values 6.335×10^{-6} Å^{-2} and -0.561×10^{-6} Å^{-2} were calculated for D_2O and H_2O, respectively, and used as a reference in the fit procedure.[53]

RESULTS AND DISCUSSION

Film Swelling. To compare the swelling behavior of PNVIBAM thin films with respect to PNIPAM thin films, polymer films of both isomers are spin-coated by using solutions with controlled polymer concentrations to obtain equivalent initial thicknesses. We prepare two sets of films (PNVIBAM and PNIPAM), which differ in their initial film thickness, namely, thick (∼130 nm) and thin (∼81 nm) films. Subsequently, as described in the Supporting Information, each film is placed in a custom-made chamber connected to a gas flow setup to enable humidity control of the sample environment. The whole SR experiment is performed at a constant temperature of ca. 19 °C, maintained and monitored by a circulating water bath. All films were dried under N_2 for 1 h before being exposed to a continuous flow of 1 L/min of DI H_2O vapor. The thickness evolution is probed with SR with a time resolution of 10 s (see Figure 2). The immediate thickness increase observed in Figure 2 is attributed to water sorption of the films. The absorption of surrounding water causes the films to expand vertically to the substrate. The thick films reach final thicknesses of 162.3 ± 0.1 nm for PNIPAM and 151.1 ± 0.1 nm for PNVIBAM, respectively (Figure 2a). The thin films swell to final thicknesses of 99.3 ± 0.1 nm for PNIPAM and 95.1 ± 0.1 nm for PNVIBAM, respectively (Figure 2a). Notably, the PNIPAM films reach higher thicknesses for both sets of films. The swelling curves are further normalized to exclude the impact of the slight differences in the initial thicknesses (see Figure S1), which shows the swelling ratio $d(t)/d_{ini}$, where $d(t)$ is the thickness measured at a given time t of the experiment and d_{ini} is the initial thickness recorded after exposing the sample to a N_2 atmosphere for 1 h. Hence, PNIPAM has a higher swelling capacity and higher water storage ability than PNVIBAM in the studied film thickness regime despite the lower LCST of PNIPAM. The difference in thickness in the fully swollen state between both isomers appears more pronounced in the thicker films depicted in Figure 2a. This observation suggests a correlation with the amount of polymer deposited on the substrate. The sterical interactions in PNIPAM and PNVIBAM films seem to affect the water sorption process, resulting in different water uptakes.

Molecular Scale Investigation. FT-IR spectroscopy is applied to probe the molecular interactions between the polymers and water during the swelling process. These measurements are performed under a constant temperature of 19 °C and after 1 h under a N_2 stream. The observed mid-infrared absorption bands of the PNIPAM film in the dry state are shown in Figure S2a. The characteristic peaks of the amide functional group are known to be the stretching absorption band of the intermolecular −N−H bond, sometimes referred to as amide A, observed here at ν(N−H) = 3300 cm^{-1}, and the amide I band related to stretching vibrations of the −C═O bond found at ν(C═O) = 1650 cm^{-1}.[54,55] The other infrared contribution of the amide group is observed at 1540 cm^{-1}, known as the amide II band, which is a coupled vibrational mode of the stretching vibrations of the −C−N bond and the bending vibrations of the −N−H bond.[54,55] In addition, the symmetric and asymmetric stretching bands of the methyl −C−H bond from the isopropyl group are identified at ν_{sym}(C−H$_3$) = 2870 cm^{-1} and ν_{as}(C−H$_3$) = 2970 cm^{-1}.[54,55] The methylene moiety of the polymer backbone of the polymer contributes to the spectrum with the asymmetric vibrations of its −C−H bond at ν_{as}(C−H$_2$) = 2930 cm^{-1} and the asymmetric bending vibrations of the −C−H at δ_{as}(C−H$_2$) = 1460 cm^{-1}.[54,55] The broad absorption peak found at 3500 cm^{-1} is attributed to the intermolecular −O−H bonded stretching vibrations, ν(O−H).[54,55] The presence of water in the FT-IR spectrum of PNIPAM after the sample had dried is a known feature of this polymer hydrogel. Indeed, PNIPAM retains water traces intermolecularly bound to the polymer. This type of water, sometimes called primary water, is attributed to strong H-bond interactions between PNIPAM and H_2O.[56−58] Figure S2b shows the IR spectrum for PNVIBAM recorded under the same conditions as the PNIPAM sample, namely, after drying. Interestingly, this spectrum does not exhibit the characteristic water absorption peak located at 3500 cm^{-1}. Thus, PNVIBAM does not retain water in its structure after drying the sample, i.e., PNVIBAM

https://doi.org/10.1021/acs.macromol.4c02802
Macromolecules 2025, 58, 1000−1010

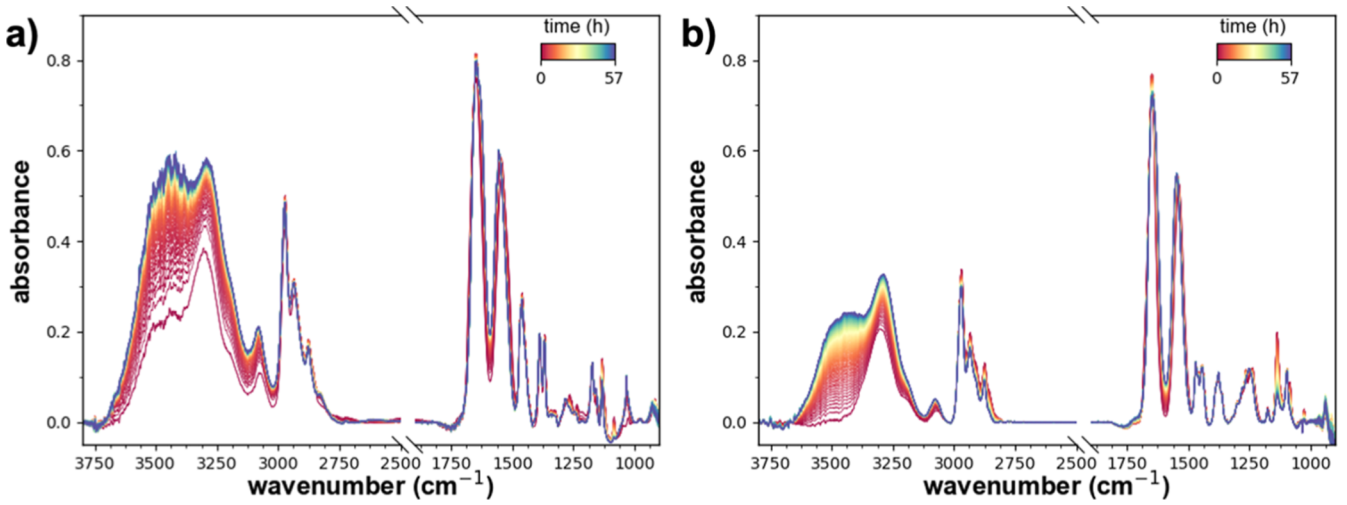

Figure 3. Temporal evolution of the FT-IR spectra during exposure to water vapor atmosphere for (a) a PNIPAM and (b) a PNVIBAM film.

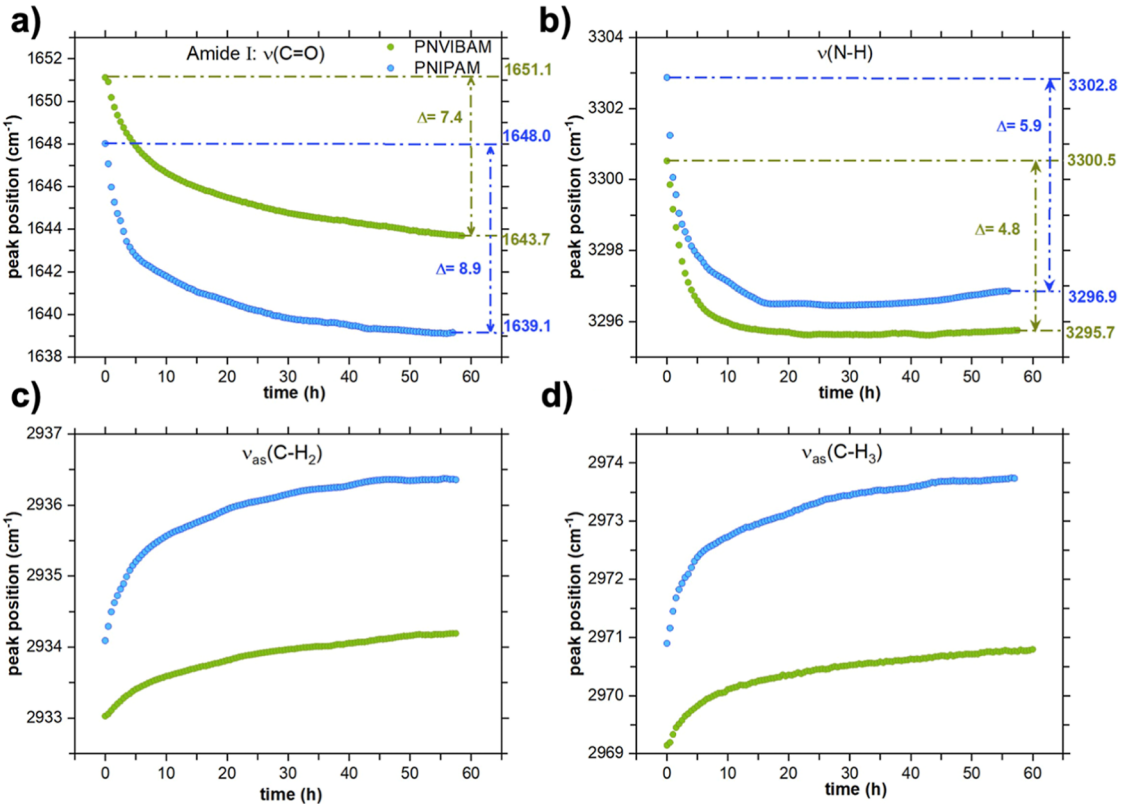

Figure 4. Peak positions of the characteristic absorbance bands of PNIPAM (blue) and PNVIBAM (green) in thin films. Peak position over time of the (a) amide I band, (b) ν(N−H) band, (c) methylene ν_{as}(C−H$_2$) band, and (d) methyl ν_{as}(C−H$_3$) band.

does not exhibit the same strong interaction with water as PNIPAM, leading to a dehydrated sample at the initial state of the experiment. The lack of primary water was previously observed for volume samples and attributed to the stronger intermolecular aggregation force within PNVIBAM chains.[43,47] Else, the characteristic peaks of the PNVIBAM moieties are observed in the FT-IR spectrum, as labeled in Figure S2b. In situ FT-IR spectra are recorded during water vapor exposure to elucidate the molecular mechanisms of the swelling process of PNVIBAM. Due to the limited time resolution of the FT-IR setup, the kinetics of the swelling process are deliberately slowed down compared to the one used for the SR characterizations. The in situ FT-IR measurements are performed for 57 h. The recorded FT-IR spectra of PNIPAM and PNVIBAM are shown in Figure 3. The spectra are plotted after background correction and atmospheric compensation. Both spectra were normalized by taking their first recorded spectrum and adjusting their absorbance on the same value for the amide I bands. For both polymers, it is seen that the water peak located at 3500 cm^{-1} grows over time, demonstrating the sorption of the surrounding water by PNIPAM and PNVIBAM. In agreement with the film swelling behavior, for PNIPAM, the water peak grows more strongly compared with PNVIBAM. The interactions of the incorporated solvent with

https://doi.org/10.1021/acs.macromol.4c02802
Macromolecules 2025, 58, 1000−1010

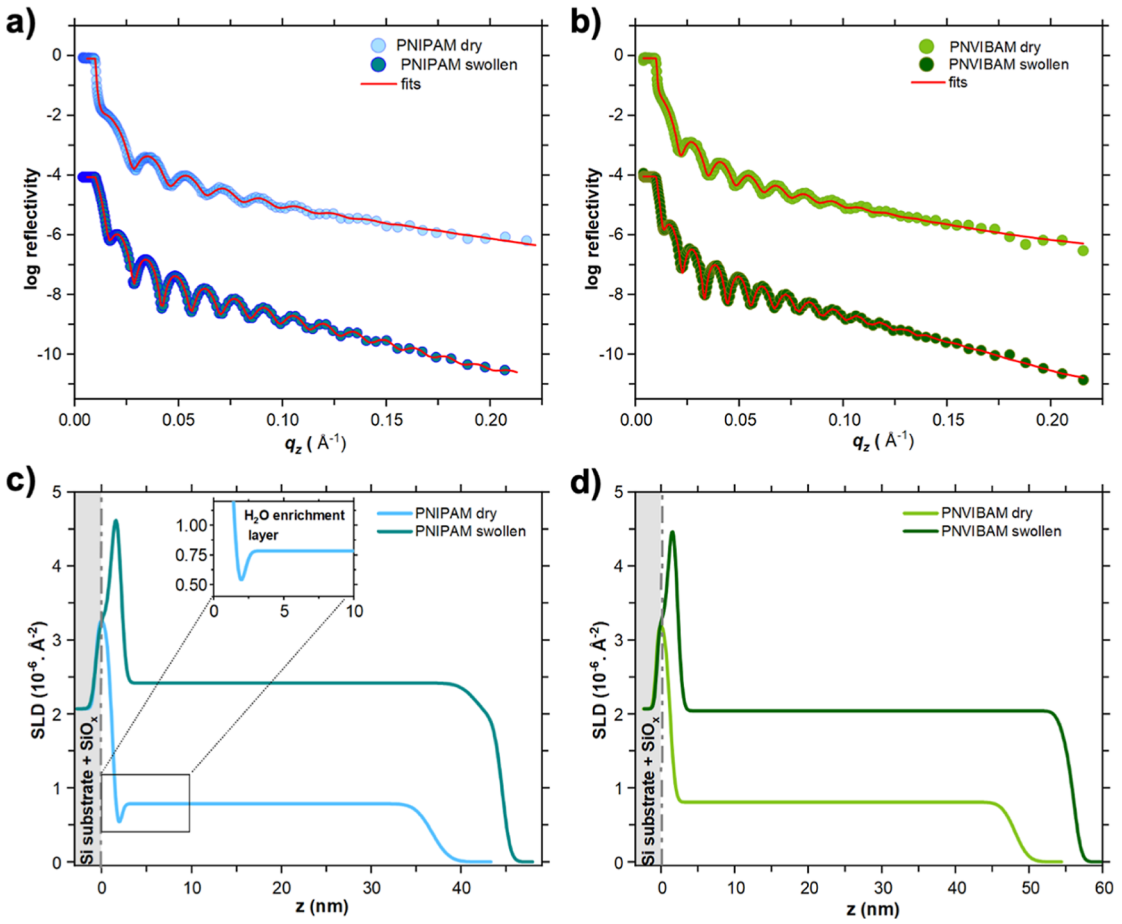

Figure 5. Static ToF-NR data (symbols) of (a) PNIPAM and (b) PNVIBAM films with fits (red solid lines), and the corresponding SLD profiles of (c) PNIPAM and (d) PNVIBAM films in the dry state (lighter color) and in the swollen state (darker color). Gray areas in the SLD plots represent the substrate of the films.

the polymeric structures are characterized by fits to the characteristic absorbance peaks using a Gaussian function and tracking the position of the centroid of these peaks over time.

Figure 4a,b shows the evolution of the peak positions of the absorbance bands of the bonds responsible for the hydrophilicity of the polymers, namely, the carbonyl and the amine moieties.[25,55,59] It is noticeable that for both polymers, the wavenumbers of the amide I and the −N−H stretching absorption bands decrease over time. This decrease in the oscillation frequency results from the bonding of new entities to these functional groups, in the present case, the formation of hydrogen bonds. The latter behavior is known for PNIPAM during hydration[25,59] and also present for PNVIBAM. However, Figure 4a shows that the shifts between the initial and the final position of −C═O bands (amide I) of the studied polymers are different. The amide I signal position of PNIPAM undergoes a shift of $\Delta = -8.9$ cm^{-1}, while the position of the amide I band in the PNVIBAM sample changes by only $\Delta = -7.4$ cm^{-1}. The strength of the hydrogen bonding to an amide group is known to correlate with the frequency of its −C═O vibration mode because the stronger the hydrogen bonding involving the carbonyl of the amide, the lower the electron density along the −C═O bond and the lower the −C═O frequency.[60] Hence, the weaker shift of the amide I signal of PNVIBAM shows that the amide I group of PNVIBAM forms weaker hydrogen bonds than PNIPAM. Regarding the ν(N−H) peak (Figure 4b), both the peaks of PNIPAM and PNVIBAM have different initial and final positions. The shift between the final and initial positions of the ν(N−H) peak in PNIPAM is $\Delta = -5.9$ cm^{-1}, while the one in PNVIBAM is $\Delta = -4.8$ cm^{-1}. Consequently, the −N−H bonds of PNIPAM, which undergo a stronger IR shift, appear to interact more with water than PNVIBAM. Accordingly, PNIPAM seems to behave more hydrophilic than PNVIBAM, despite its LCST. The differences in interaction energies could explain such a scenario: in the polymer-rich region of the phase diagram, the interaction energy between the polymer chains seems to be higher for PNVIBAM compared to PNIPAM, whereas, in the solvent-rich region, the interaction energy between the polymer and water appears to be also higher for PNVIBAM than for PNIPAM. As the presented study focuses on thin film configuration, the depicted behavior has to be considered within the polymer-rich part of the phase diagram.

The evolution of the peak positions of the functional groups responsible for the hydrophobic behavior is shown in Figures 4c,d and S3 in the Supporting Information. These three graphs exhibit shifts of the methylene ν_{as}(C−H_2), the methyl ν_{as}(C−H_3) bands from the isopropyl groups, and the amide II bands of PNIPAM and PNVIBAM. The peak of those entities shifts toward higher wavenumbers. This increase in the vibration frequency is characteristic of a water clathrate around these hydrophobic groups. This behavior is characteristic of PNIPAM systems. Below the LCST, the enthalpic contribu-

https://doi.org/10.1021/acs.macromol.4c02802
Macromolecules 2025, 58, 1000−1010

tions from hydrogen bonding between amide groups and water molecules stabilize PNIPAM in its hydrated and elongated state. These enthalpic effects dominate the entropic contributions of the hydrophobic isopropyl groups, which are surrounded by a stable water clathrate structure.[31,61−65] The hydrophobic interactions between water and these bonds lead to a confinement of the vibrational motions of the considered bonds, resulting in a shift of the peaks toward higher wavenumbers. In both cases, the shift of the peaks of PNIPAM is more pronounced than that of the peaks of PNVIBAM. Thus, PNIPAM seems to exhibit stronger confinement from the water clathrates than PNVIBAM, which appears to have larger water cages. The rearrangement of the amide II peak (Figure S3) during the water exposure suffers from the same confinement, leading to a shift to higher wavenumbers. Furthermore, the PNIPAM amide II absorbance band reaches a higher wavenumber value than that of PNVIBAM, demonstrating a stronger confinement. This observation correlates with the hypothetical smaller water cages present in PNIPAM. Consequently, PNIPAM appears to have a stronger affinity for water than PNVIBAM, as it presents stronger hydrophilic interactions. The presence of large water clathrates arising from the hydrophobic interactions in PNVIBAM seems to repel water and sterically hinder the introduction of free water molecules within the polymer thin film. This behavior can explain the observed reduced swelling of PNVIBAM films compared to PNIPAM films, as revealed by SR (Figure 2).

Depth Profiling Investigation. The distribution of the components along the surface normal of the polymer thin films is investigated with ToF-NR. Neutrons allow precise depth profiling of the hydrated polymer thin films without causing beam damage. An accurate investigation is enabled by choosing D_2O as a solvent for the swelling measurements, as it has a high SLD, resulting in a strong scattering contrast between the solvent and the polymer. To obtain detailed knowledge of the solvent distribution at the initial and final stages of the swelling process, ToF-NR static measurements are performed in the N_2-stream dried and D_2O hydrated (swollen) states, also called static measurements. In addition, time-resolved ToF-NR measurements, also called kinetic measurements, are performed to assess the D_2O uptake over time and the resulting thickness increase of the films. The static measurements are recorded at two incident angles to access reflectivity data within a large q_z range. The obtained data from the specular reflectivity are fitted with a layered structure model to replicate the polymer film configurations. Detailed settings of the measurement and the models used are provided in the Supporting Information. Besides the observed reflectivity fringes, the associated SLD profiles determined from the fits give a comprehensive view of the solvent distribution within the films. Figure 5 shows the respective dry and swollen static ToF-NR measurements of the PNIPAM and PNVIBAM films and their respective SLD profiles.

Figure 5a,b shows that, in both films, the critical edge shifts toward higher q_z values in the swollen states compared to the dry states. This shift originates from an increase in the SLD of the overall films, suggesting the incorporation of D_2O, as the solvent has a higher SLD than do the polymers. Additionally, the swelling of the films is evidenced by the narrowing of the Kiessig fringes compared to the dry state, revealing significant structural alterations induced by hydration. As determined from the model fits, the initial film thickness in the dry state is 37 ± 1 nm for PNIPAM and 48 ± 1 nm for PNVIBAM film, respectively. The derived SLD profiles are depicted in Figure 5c,d, in dependence on z, the distance to the substrate in the direction normal to the substrate surface. In the case of the PNIPAM film, the dry state ToF-NR data can only be fitted with a three-layer model, which includes an interface layer to the substrate, the main polymer layer, and an interface layer toward the air. The Si substrate and the native SiO_x layer originating from the substrate cleaning procedure are not counted since their parameters are kept constant in the fits as they are not expected to change during the experiment. A detailed description of the generic layer models presented in this study can be found in the Supporting Information. The main polymer layer has a SLD value of 0.78×10^{-6} Å^{-2}, which is slightly below the theoretical SLD value of PNIPAM. As illustrated in the inset plot of Figure 5c, there is a distinct drop in the SLD profile close to the substrate in the dry state. In addition, the surface enrichment layer has a lower SLD as well. The presence of H_2O can explain these observations as H_2O has a negative neutron SLD of -0.561×10^{-6} Å^{-2}. Therefore, the decrease in the SLD is attributed to the presence of primary water, which is also found in the FT-IR characterizations. This enrichment layer results from the Si substrate acid cleaning procedure plus the O_2 plasma treatment, which ensures a hydrophilic surface of the substrate by forming a SiO_x layer that creates polar silanol groups (−Si−OH) via hydrogen bonding with the residual water in the polymeric system. In addition, neutron-based characterization techniques such as ToF-NR grant an easy contrast variation where the SLD, which depends on the probed materials' mass density and the elemental constitution, is directly measured. Hence, knowing the theoretical SLD of H_2O and the polymer enables us to attribute the SLD variations to different layers and interfaces. Thus, both techniques, FT-IR and ToF-NR, consistently reveal the presence of water in the PNIPAM film, even after the film has been dried under N_2 for 1 h. Furthermore, combining two neutron incident angles for the static ToF-NR measurements leads to the coverage of a broad range of momentum transfers, q_z, enabling a high-resolution determination of the whole vertical film distribution. Thus, ToF-NR completes the FT-IR findings, revealing that this residual water is not homogeneously distributed but enriched at both interfaces, substrate−film and film-atmosphere. In contrast, the ToF-NR data of the PNVIBAM film, shown in Figure 5b, can be fitted with a two-layer model, namely, the main polymer layer and the polymer−air interface layer. The SLD profile resulting from this fit is shown in Figure 5d. The main polymer layer again has a SLD value of 0.78×10^{-6} Å^{-2}, which is slightly below the expected SLD value of PNVIBAM. The surface enrichment layer has a slightly lower SLD value as well, indicating the presence of trace amounts of residual water in the entire PNVIBAM film. The absence of a water-rich region near the substrate agrees well with the FT-IR analysis. The detection of traces of primary water with ToF-NR might originate from the different film thicknesses. Indeed, thicker films are needed to record strong enough IR absorbance. For the swollen film states, the ToF-NR data are fitted with a similar model structure consisting of layers. In both cases, the SLD values increase drastically at the substrate−polymer interface. This observation is attributed to a D_2O enrichment layer, as D_2O has the highest SLD value. Also, the main polymer layers show a higher SLD value than the SLD obtained in the dried state due to the D_2O incorporation

https://doi.org/10.1021/acs.macromol.4c02802
Macromolecules 2025, 58, 1000−1010

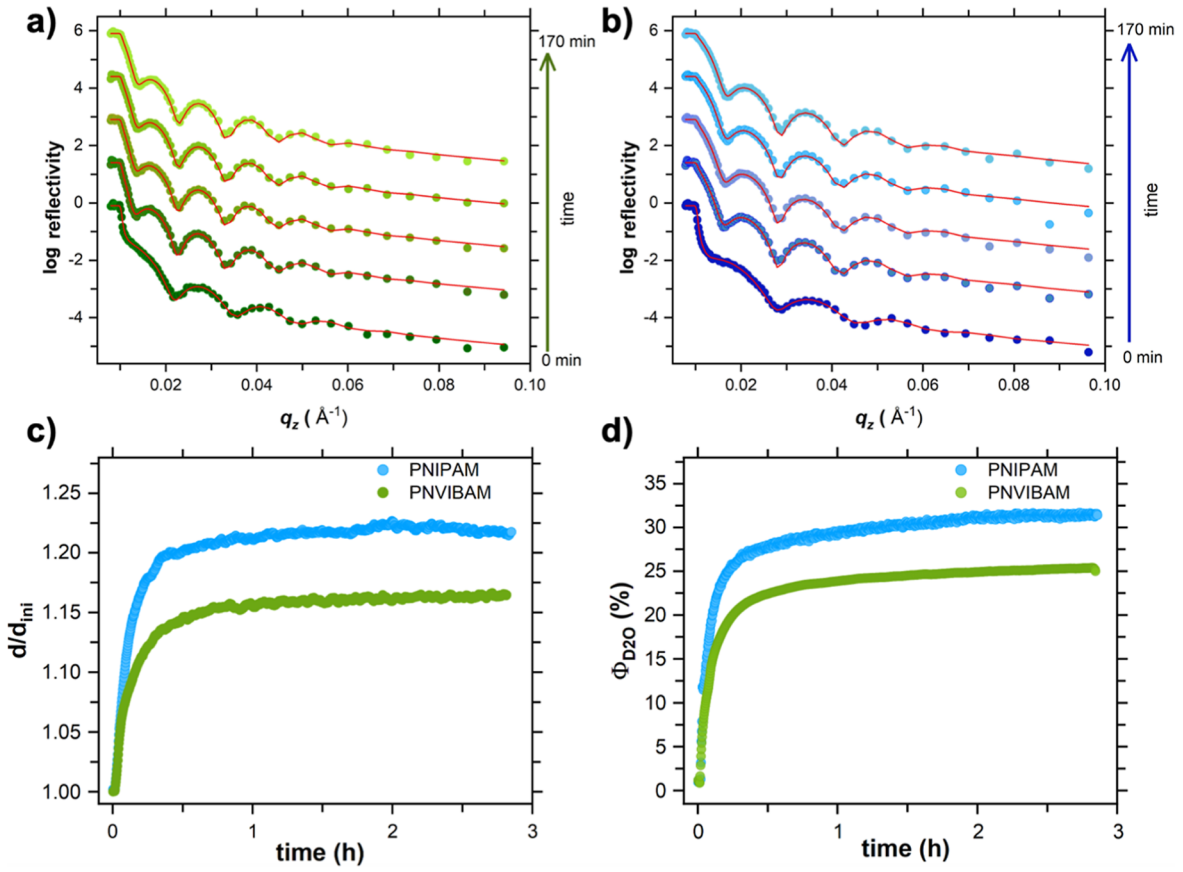

Figure 6. Selection of ToF-NR data recorded during the film swelling in D_2O vapor atmosphere for (a) PNVIBAM and (b) PNIPAM films. Curves are shifted along the vertical axis with time for clarity of the presentation. Solid red lines show the model fits. Temporal evolution of (c) the swelling ratio and (d) volume fraction of D_2O of the main polymer layer for PNIPAM (blue) and PNVIBAM (green) films.

within the polymer layer. In the case of PNVIBAM, the SLD value of the main polymer layer reaches 2.04×10^{-6} Å^{-2}, whereas for PNIPAM, it reaches 2.40×10^{-6} Å^{-2}, indicating a different uptake of D_2O, as in both samples, the main polymer layer has the same SLD value. Considering that the investigated PNIPAM film was initiated with a smaller thickness than the PNVIBAM film, the observed SLD difference agrees with a higher hydrophilicity of the PNIPAM film. Once equilibrated, the PNVIBAM film swells up to a thickness of 57 ± 1 nm and the PNIPAM to 44 ± 1 nm.

In addition to the static measurement, kinetic ToF-NR measurements are recorded to obtain insights into the swelling processes during exposure to a D_2O vapor atmosphere. Figure 6 illustrates the observed changes in the ToF-NR data during solvent uptake. As seen with the statics measurements, a narrowing of the fringes during the swelling process is observed, indicating a thickness increase with the solvent absorption. The data of the kinetic measurements are fitted with a two-layer model consisting of the D_2O enrichment layer at the substrate and the main polymer layer (see Supporting Information). The parameters describing the substrate with its native SiO_x layer are kept constant during the fit procedure. A two-layer model is chosen as the kinetic ToF-NR measurements are performed at only one neutron incident angle, resulting in a narrower q-range than that of the static measurements. In fact, reducing the q-range enables a higher time resolution, allowing the study of fast swelling processes, but it limits the number of fit parameters. The resulting kinetic ToF-NR characterization is studied with a time resolution of 10.55 s, comparable to the SR measurements' probing time. The validity of the reduced layer model is verified with the fit parameters of the dry and hydrated state of the sample, which represents the initial and final states of the characterization and therefore sets the limit of the fit parameters in the time-resolved study. Figure 6c shows the temporal evolution of swelling ratio $d(t)/d_{ini}$. Figure 6d shows the time evolution of the increase in the volume fraction of D_2O, written as Φ_{D2O}, extracted from the fits for the main polymer layer. Figure 6c reveals that the PNIPAM main layer undergoes an expansion of 22%, while for PNVIBAM, it is 16%. Thus, PNVIBAM reaches a swelling ratio smaller than that of PNIPAM, matching the SR results described above. The uptake of solvent is determined from the time-evolution of the volume fraction of D_2O[12,13]

$$\Phi_{D2O}(t) = \frac{SLD_{meas}(t) - SLD_{poly}}{SLD_{D2O} - SLD_{poly}}$$

where $SLD_{meas}(t)$ is the SLD of the main polymer layer at a given time t of the swelling process, SLD_{poly} is the SLD of the dry polymer, and SLD_{D2O} is the SLD of neat D_2O. $\Phi_{D2O}(t)$ is calculated only from the SLD rise of the main polymer layer. Therefore, the affinity of water with the isomers is decoupled from the enrichment layer present at the substrate−polymer, which is driven by the interaction with the substrate. Figure 6d shows that the D_2O volume fraction in the PNIPAM main layer is 31%, while the PNVIBAM polymer main layer reaches only a volume fraction of 25%. Hence, the PNIPAM film takes

https://doi.org/10.1021/acs.macromol.4c02802
Macromolecules 2025, 58, 1000−1010

up more D_2O than the PNVIBAM film, in agreement with the observations from the SR and FT-IR measurements.

The overall swelling of the main polymer layer within the films is further characterized by plotting the dependence of the film thickness vs the D_2O content, as illustrated in Figure 7.

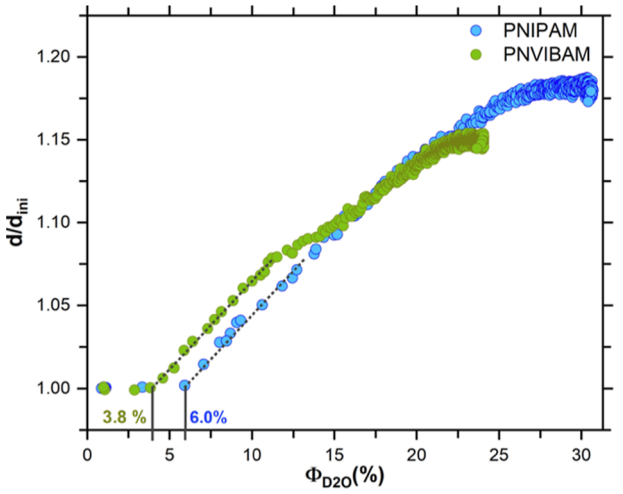

Figure 7. Evolution of the swelling ratio versus the solvent content expressed as the volume fraction of D_2O for PNIPAM and PNVIBAM films. Dotted lines are linear fits. Solid lines extrapolate to the water uptake without film swelling.

Two major hydration different regimes are detected. The first regime is characterized by water uptake without film swelling, and the second regime shows film swelling during water uptake. For the second regime, the parallel dotted gray lines with similar slopes suggest that the thickness evolution of both isomers follows a similar linear trend for the film swelling. However, the amount of solvent that was taken up to transit into this second regime depends on the polymer. Different D_2O volume fractions are required to induce film swelling. In the first regime, despite the high relative humidity conditions, both films start solvent sorption without swelling. Water molecules penetrate into the film and fill the available free volume.[66,67] With increasing amounts of incorporated water, the polymers gain mobility. They may change conformation and expand to accommodate more solvent molecules (second regime). As seen in Figure 7, in the case of PNVIBAM, a D_2O volume fraction of 3.8% is required to induce film swelling, whereas, for PNIPAM, a volume fraction of D_2O of 6.0% is needed. In other words, swelling occurs in the PNVIBAM film with a smaller amount of water than that in the PNIPAM film. A possible explanation may lie in the different glass transition temperatures of PNIPAM and PNVIBAM, as well as in a difference in the fractional free volume or its accessibility between both polymers. Indeed, a glass transition temperature of T_g = 152 °C was measured by Henschel et al. for the same PNVIBAM batch,[41] while literature gives a glass transition temperature of PNIPAM ranging from 130 to 140 °C.[68−71] This observation correlates with the presence of hydrophobic water clathrates, as found using FT-IR. Specifically, PNVIBAM seems to have larger water cages around the hydrophobic moieties of the polymer, which can sterically hinder the sorption of additional water molecules from the vapor in the free volume of the polymer film. In contrast, PNIPAM, which appears to have smaller hydration units due to the stronger confinement induced by the water clathrates, offers a larger accessible volume for the uptake of additional water from the vapor.

Regarding the temporal evolution of the water enrichment layers near the substrate, a difference in the thickness of this layer is seen in Figure S6a in the Supporting Information. In the case of PNVIBAM, the enrichment layer is slightly thicker compared with PNIPAM. Also, the enrichment layer needs a longer time to grow in thickness for PNVIBAM than for PNIPAM. In addition, a faster rise of the SLD is observed in the case of the PNVIBAM thin film as well, as shown in Figure S6b in the Supporting Information. The incorporation of D_2O at the interface between the bulk layer and the substrate drives this SLD increase. We attribute this to the presence of primary light water in PNIPAM at the interface, which slows down the uptake of deuterated water because a solvent exchange is required to replace existing protonated water with deuterated water from the vapor. The SLDs recorded in the hydrated states of both samples reach similar values, demonstrating that a comparable amount of D_2O is located at this interface in both thin films.

CONCLUSIONS

The potential of PNVIBAM, a structural isomer of PNIPAM, is explored with respect to film swelling in a water vapor atmosphere at room temperature. It turns out that the swelling behavior differs. In the final hydrated states, PNVIBAM thin films swell less than PNIPAM thin films do. Such differences in the mesoscopic film behavior result from differences on the molecular level, as seen by the FT-IR measurements. The amide I and −N−H signals, which correspond to the groups responsible for the hydrophilicity of the polymers, show less affinity for water in the case of PNVIBAM, although its LCST in solution is higher than the LCST of PNIPAM. In addition, the hydrophobic moieties of PNIPAM, the isopropyl groups, and the methylene group in the polymer backbone appear to be subject to stronger confinement from the surrounding water clathrates. In contrast, the larger water cages present in PNVIBAM imply a steric hindrance for the water molecules to access the free volume within the polymer film. Such differences in the water content also result in differences in the water distribution inside the thin films, as deduced by ToF-NR.

Along the same direction, the PNIPAM films still contain residual primary water inside the films after exposure to dry N_2 gas, while the PNVIBAM thin films are virtually completely dry, according to the FT-IR spectra.

Kinetic studies of the swelling process reveal a better understanding of the resulting final swollen films. The water uptake of the main polymer layer proceeds in two steps. Initially, the water molecules only fill the free volume of the films, until in the second stage, the water uptake is accompanied by an increase in the film thickness. The PNVIBAM film reaches the transition into the film swelling at a lower water amount incorporated compared to the PNIPAM film. Regarding the water enrichment layer near the substrate, the exchange from protonated water to deuterated water is driving the kinetics at this interface in the PNIPAM film, while the PNVIBAM film shows a fast uptake of D_2O.

In summary, the higher LCST of PNVIBAM in water makes this polymer attractive as a substitute for PNIPAM. The study of the response of these isomers to water vapor exposure gives a better understanding of PNVIBAM behavior, widening the choice of LCST-type polymers for various applications. The

https://doi.org/10.1021/acs.macromol.4c02802
Macromolecules 2025, 58, 1000−1010

observed differences underline that an exchange of PNIPAM with PNVIBAM will give rise to differences in the behavior, which need to be considered when applying it in drug delivery systems, biosensors, actuators, and responsive coatings.

■ ASSOCIATED CONTENT

Supporting Information

The Supporting Information is available free of charge at https://pubs.acs.org/doi/10.1021/acs.macromol.4c02802.

PNVIBAM description and polymerization; sample environment description; FT-IR spectrometer configuration and measurement parameters; details on the used polymer concentrations; PNIPAM and PNVIBAM swelling ratios; PNIPAM and PNVIBAM dry mid-IR spectra; peak shift for IR amide II bands ToF-NR instrument configuration and measurement parameters; data reduction; modeled reflectivity from batch fitting kinetic ToF-NR data; and batch fitting kinetics ToF-NR of the polymer substrate interface (PDF)

■ AUTHOR INFORMATION

Corresponding Author

Peter Müller-Buschbaum − *TUM School of Natural Sciences, Department of Physics, Chair for Functional Materials, Technical University of Munich, 85748 Garching, Germany;* orcid.org/0000-0002-9566-6088; Phone: +49 89 289 12451; Email: muellerb@ph.tum.de; Fax: +49 89 12473

Authors

Morgan P. Le Dû − *TUM School of Natural Sciences, Department of Physics, Chair for Functional Materials, Technical University of Munich, 85748 Garching, Germany;* orcid.org/0000-0002-5879-1461

Julija Reitenbach − *TUM School of Natural Sciences, Department of Physics, Chair for Functional Materials, Technical University of Munich, 85748 Garching, Germany;* orcid.org/0000-0001-8142-7337

David P. Kosbahn − *TUM School of Natural Sciences, Department of Physics, Chair for Functional Materials, Technical University of Munich, 85748 Garching, Germany;* orcid.org/0000-0001-8632-2059

Lukas V. Spanier − *TUM School of Natural Sciences, Department of Physics, Chair for Functional Materials, Technical University of Munich, 85748 Garching, Germany;* orcid.org/0000-0003-0300-2987

Robert Cubitt − *Institut Laue-Langevin, 38042 Grenoble, France*

Cristiane Henschel − *Institut für Chemie, Universität Potsdam, 14476 Potsdam-Golm, Germany*

André Laschewsky − *Institut für Chemie, Universität Potsdam, 14476 Potsdam-Golm, Germany; Fraunhofer Institut für Angewandte Polymerforschung, 14476 Potsdam-Golm, Germany;* orcid.org/0000-0003-2443-886X

Christine M. Papadakis − *TUM School of Natural Sciences, Department of Physics, Soft Matter Physics Group, Technical University of Munich, 85748 Garching, Germany;* orcid.org/0000-0002-7098-3458

Complete contact information is available at: https://pubs.acs.org/10.1021/acs.macromol.4c02802

Author Contributions

The manuscript was written through the contributions of all authors. All authors have given their approval to the final version of the manuscript.

Funding

We thank Deutsche Forschungsgemeinschaft (DFG) for financial support (LA 611/16-1, MU 1487/29-1, PA 771/20-1) and the German Ministry for Education and Research (BMBF) for funding via the project "FlexiProb" (grant no. 05 K2016).

Notes

The authors declare no competing financial interest.

■ ACKNOWLEDGMENTS

Institut Laue-Langevin and the neutron reflectometer D17 are acknowledged for beam time allocation and providing excellent equipment and support of measurements.

■ REFERENCES

(1) Wei, M.; Gao, Y.; Li, X.; Serpe, M. J. Stimuli-responsive polymers and their applications. *Polym. Chem.* **2017**, *8* (1), 127−143.

(2) Aguilar, M. R.; San Román, J. Chapter 1 - Introduction to Smart Polymers and Their Applications. In *Smart Polymers and their Applications*, 2nd ed.; Aguilar, M. R., San Román, J., Eds.; Woodhead Publishing, 2019; pp 1−11.

(3) Wang, S.; Liu, Q.; Li, L.; Urban, M. W. Recent Advances in Stimuli-Responsive Commodity Polymers. *Macromol. Rapid Commun.* **2021**, *42* (18), 2100054.

(4) Png, Z. M.; Wang, C.-G.; Yeo, J. C. C.; Lee, J. J. C.; Surat'man, N. E.; Tan, Y. L.; Liu, H.; Wang, P.; Tan, B. H.; Xu, J. W.; et al. Stimuli-responsive structure−property switchable polymer materials. *Mol. Syst. Des. Eng.* **2023**, *8* (9), 1097−1129.

(5) Tariq, A.; Arif, Z. U.; Khalid, M. Y.; Hossain, M.; Rasool, P. I.; Umer, R.; Ramakrishna, S. Recent Advances in the Additive Manufacturing of Stimuli-Responsive Soft Polymers. *Adv. Eng. Mater.* **2023**, *25* (21), 2301074.

(6) García-Fernández, L.; Mora-Boza, A.; Reyes-Ortega, F. Chapter 3 - pH-Responsive Polymers: Properties, Synthesis, and Applications. In *Smart Polymers and their Applications*, 2nd ed.; Aguilar, M. R., San Román, J., Eds.; Woodhead Publishing, 2019; pp 45−86.

(7) Xiong, X.; del Campo, A.; Cui, J. Chapter 4 - Photoresponsive Polymers. In *Smart Polymers and their Applications*, 2nd ed.; Aguilar, M. R., San Román, J., Eds.; Woodhead Publishing, 2019; pp 87−153.

(8) Manouras, T.; Vamvakaki, M. Field responsive materials: photo-, electro-, magnetic- and ultrasound-sensitive polymers. *Polym. Chem.* **2017**, *8* (1), 74−96.

(9) Hoogenboom, R. Chapter 2 - Temperature-Responsive Polymers: Properties, Synthesis, and Applications. In *Smart Polymers and their Applications*, 2nd ed.; Aguilar, M. R., San Román, J., Eds.; Woodhead Publishing, 2019; pp 13−44.

(10) Suwa, K.; Yamamoto, K.; Akashi, M.; Takano, K.; Tanaka, N.; Kunugi, S. Effects of salt on the temperature and pressure responsive properties of poly(N-vinylisobutyramide) aqueous solutions. *Colloid Polym. Sci.* **1998**, *276* (6), 529−533.

(11) Scherzinger, C.; Schwarz, A.; Bardow, A.; Leonhard, K.; Richtering, W. Cononsolvency of poly-N-isopropyl acrylamide (PNIPAM): Microgels versus linear chains and macrogels. *Curr. Opin. Colloid Interface Sci.* **2014**, *19* (2), 84−94.

(12) Geiger, C.; Reitenbach, J.; Kreuzer, L. P.; Widmann, T.; Wang, P.; Cubitt, R.; Henschel, C.; Laschewsky, A.; Papadakis, C. M.; Müller-Buschbaum, P. PMMA-b-PNIPAM Thin Films Display Cononsolvency-Driven Response in Mixed Water/Methanol Vapors. *Macromolecules* **2021**, *54* (7), 3517−3530.

(13) Reitenbach, J.; Geiger, C.; Wang, P.; Vagias, A.; Cubitt, R.; Schanzenbach, D.; Laschewsky, A.; Papadakis, C. M.; Müller-Buschbaum, P. Effect of Magnesium Salts with Chaotropic Anions

on the Swelling Behavior of PNIPMAM Thin Films. *Macromolecules* **2023**, *56* (2), 567−577.
(14) Duro-Castano, A.; Talelli, M.; Rodríguez-Escalona, G.; Vicent, M. J. Chapter 13 - Smart Polymeric Nanocarriers for Drug Delivery. In *Smart Polymers and their Applications*, 2nd ed.; Aguilar, M. R., San Román, J., Eds.; Woodhead Publishing, 2019; pp 439−479.
(15) Bauri, K.; Nandi, M.; De, P. Amino acid-derived stimuli-responsive polymers and their applications. *Polym. Chem.* **2018**, *9* (11), 1257−1287.
(16) Aggas, J. R.; Guiseppi-Elie, A. 2.5.13 - Responsive Polymers in the Fabrication of Enzyme-Based Biosensors. In *Biomaterials Science*, 4th ed.; Wagner, W. R., Sakiyama-Elbert, S. E., Zhang, G., Yaszemski, M. J., Eds.; Academic Press, 2020; pp 1267−1286.
(17) Couturier, J.-P.; Sütterlin, M.; Laschewsky, A.; Hettrich, C.; Wischerhoff, E. Responsive Inverse Opal Hydrogels for the Sensing of Macromolecules. *Angew. Chem., Int. Ed.* **2015**, *54* (22), 6641−6644.
(18) Krishnamoorthy, M.; Hakobyan, S.; Ramstedt, M.; Gautrot, J. E. Surface-initiated polymer brushes in the biomedical field: applications in membrane science, biosensing, cell culture, regenerative medicine and antibacterial coatings. *Chem. Rev.* **2014**, *114* (21), 10976−11026.
(19) Nagappan, S.; Moorthy, M. S.; Rao, K. M.; Ha, C.-S. Stimuli-Responsive Smart Polymeric Coatings: An Overview. In *Industrial Applications for Intelligent Polymers and Coatings*; Hosseini, M., Makhlouf, A. S. H., Eds.; Springer International Publishing, 2016; pp 27−49.
(20) Maeda, Y.; Higuchi, T.; Ikeda, I. Change in Hydration State during the Coil−Globule Transition of Aqueous Solutions of Poly(N-isopropylacrylamide) as Evidenced by FTIR Spectroscopy. *Langmuir* **2000**, *16* (19), 7503−7509.
(21) Hua, L.; Xie, M.; Jian, Y.; Wu, B.; Chen, C.; Zhao, C. Multiple-Responsive and Amphibious Hydrogel Actuator Based on Asymmetric UCST-Type Volume Phase Transition. *ACS Appl. Mater. Interfaces* **2019**, *11* (46), 43641−43648.
(22) Wang, C.; Hashimoto, T. Time-Resolved Light Scattering of Atactic Poly (*N*-isopropylacrylamide) in Water: Physical Gelation and Spinodal Temperature of the Hydrogel. *Macromolecules* **2024**, *57*, 5398−5408.
(23) Wang, C.; Hashimoto, T.; Chuang, Y.-C.; Tanaka, K.; Chang, Y.-P.; Yang, T.-W.; Huang, M.-T. Physical gelation of aqueous solutions of atactic poly (N-isopropylacrylamide). *Macromolecules* **2022**, *55* (20), 9152−9167.
(24) He, C.; Kim, S. W.; Lee, D. S. In situ gelling stimuli-sensitive block copolymer hydrogels for drug delivery. *J. Controlled Release* **2008**, *127* (3), 189−207.
(25) Tamai, Y.; Tanaka, H.; Nakanishi, K. Molecular Dynamics Study of Polymer−Water Interaction in Hydrogels. 1. Hydrogen-Bond Structure. *Macromolecules* **1996**, *29* (21), 6750−6760.
(26) Schmaljohann, D. Thermo-responsive polymers and hydrogels in tissue engineering. *e-Polym.* **2005**, *5* (1), 021.
(27) Tokarev, I.; Minko, S. Stimuli-responsive hydrogel thin films. *Soft Matter* **2009**, *5* (3), 511−524.
(28) Montero, A.; Valencia, L.; Corrales, R.; Jorcano, J. L.; Velasco, D. Chapter 9 - Smart Polymer Gels: Properties, Synthesis, and Applications. In *Smart Polymers and their Applications*, 2nd ed.; Aguilar, M. R., San Román, J., Eds.; Woodhead Publishing, 2019; pp 279−321.
(29) Halperin, A.; Kröger, M.; Winnik, F. M. Poly(N-isopropylacrylamide) Phase Diagrams: Fifty Years of Research. *Angew. Chem., Int. Ed.* **2015**, *54* (51), 15342−15367.
(30) Papadakis, C. M.; Niebuur, B.-J.; Schulte, A. Thermoresponsive Polymers under Pressure with a Focus on Poly (N-isopropylacrylamide)(PNIPAM). *Langmuir* **2024**, *40* (1), 1−20.
(31) Cho, E. C.; Lee, J.; Cho, K. Role of Bound Water and Hydrophobic Interaction in Phase Transition of Poly(N-isopropylacrylamide) Aqueous Solution. *Macromolecules* **2003**, *36* (26), 9929−9934.
(32) Deshmukh, S. A.; Sankaranarayanan, S. K. R. S.; Suthar, K.; Mancini, D. C. Role of Solvation Dynamics and Local Ordering of Water in Inducing Conformational Transitions in Poly(N-isopropylacrylamide) Oligomers through the LCST. *J. Phys. Chem. B* **2012**, *116* (9), 2651−2663.
(33) Vihola, H.; Laukkanen, A.; Valtola, L.; Tenhu, H.; Hirvonen, J. Cytotoxicity of thermosensitive polymers poly(*N*-isopropylacrylamide), poly(*N*-vinylcaprolactam) and amphiphilically modified poly(*N*-vinylcaprolactam). *Biomaterials* **2005**, *26* (16), 3055−3064.
(34) Campos, E.; Almirall, M.; Mtnez-Almela, J.; Palatsi, J.; Flotats, X. Feasibility study of the anaerobic digestion of dewatered pig slurry by means of polyacrylamide. *Bioresour. Technol.* **2008**, *99* (2), 387−395.
(35) Pennisi, M.; Malaguarnera, G.; Puglisi, V.; Vinciguerra, L.; Vacante, M.; Malaguarnera, M. Neurotoxicity of Acrylamide in Exposed Workers. *Int. J. Environ. Res. Public Health* **2013**, *10* (9), 3843−3854.
(36) Cortez-Lemus, N. A.; Licea-Claverie, A. Poly(N-vinylcaprolactam), a comprehensive review on a thermoresponsive polymer becoming popular. *Prog. Polym. Sci.* **2016**, *53*, 1−51.
(37) Yoshida, H.; Furumai, H.; Ajiro, H. Preparation and Characterization of Thermoresponsive Poly(N-vinylisobutyramide) Microgels. *Langmuir* **2022**, *38* (17), 5269−5274.
(38) Ramos, J.; Imaz, A.; Forcada, J. Temperature-sensitive nanogels: poly(N-vinylcaprolactam) versus poly(N-isopropylacrylamide). *Polym. Chem.* **2012**, *3* (4), 852−856.
(39) Liu, J.; Debuigne, A.; Detrembleur, C.; Jérôme, C. Poly(N-vinylcaprolactam): A Thermoresponsive Macromolecule with Promising Future in Biomedical Field. *Adv. Healthcare Mater.* **2014**, *3* (12), 1941−1968.
(40) Patra, L.; Messman, J. M.; Toomey, R. On the nature of volume-phase transitions in photo-cross-linked poly(cyclopropylacrylamide) and poly(*N*-vinylisobutyramide) coatings. *Soft Matter* **2013**, *9* (16), 4349−4356.
(41) Henschel, C.; Schanzenbach, D.; Laschewsky, A.; Ko, C.-H.; Papadakis, C. M.; Müller-Buschbaum, P. Thermoresponsive and co-nonsolvency behavior of poly(*N*-vinyl isobutyramide) and poly(*N*-isopropyl methacrylamide) as poly(*N*-isopropyl acrylamide) analogs in aqueous media. *Colloid Polym. Sci.* **2023**, *301* (7), 703.
(42) Kunugi, S.; Tada, T.; Tanaka, N.; Yamamoto, K.; Akashi, M. Microcalorimetric Study of Aqueous Solution of a Thermoresponsive Polymer, poly(N-vinylisobutyramide) (PNVIBA). *Polym. J.* **2002**, *34* (5), 383−388.
(43) Suwa, K.; Wada, Y.; Kishida, A.; Akashi, M. Synthesis and functionalities of poly(N-vinylalkylamide). VI. A novel thermosensitive hydrogel crosslinked poly(N-vinylisobutyramide). *J. Polym. Sci., Part A: Polym. Chem.* **1997**, *35* (16), 3377−3384.
(44) Serizawa, T.; Chen, M.-Q.; Akashi, M. Graft copolymers having hydrophobic backbone and hydrophilic branches. XVIII. Poly(styrene) nanospheres with novel thermosensitive poly(N-vinylisobutyramide)s on their surfaces. *J. Polym. Sci., Part A: Polym. Chem.* **1998**, *36* (14), 2581−2587.
(45) Marchetti, M.; Prager, S.; Cussler, E. Thermodynamic predictions of volume changes in temperature-sensitive gels. 2. Experiments. *Macromolecules* **1990**, *23* (14), 3445−3450.
(46) Suwa, K.; Morishita, K.; Kishida, A.; Akashi, M. Synthesis and functionalities of poly(*N*-vinylalkylamide). V. Control of a lower critical solution temperature of poly(*N*-vinylalkylamide). *J. Polym. Sci., Part A: Polym. Chem.* **1997**, *35* (15), 3087−3094.
(47) Suwa, K.; Wada, Y.; Kikunaga, Y.; Morishita, K.; Kishida, A.; Akashi, M. Synthesis and functionalities of poly(N-vinylalkylamide). IV. Synthesis and free radical polymerization of N-vinylisobutyramide and thermosensitive properties of the polymer. *J. Polym. Sci., Part A: Polym. Chem.* **1997**, *35* (9), 1763−1768.
(48) Aseyev, V. O.; Tenhu, H.; Winnik, F. M. Temperature Dependence of the Colloidal Stability of Neutral AmphiphilicPolymers in Water. In *Conformation-Dependent Design of Sequences in Copolymers II*; Khokhlov, A. R., Ed.; Springer Berlin Heidelberg, 2006; pp 1−85.
(49) Philipp, M.; Körstgens, V.; Magerl, D.; Heller, C.; Yao, Y.; Wang, W.; Santoro, G.; Roth, S. V.; Müller-Buschbaum, P. Sorption of

https://doi.org/10.1021/acs.macromol.4c02802
Macromolecules 2025, 58, 1000−1010

Water and Initial Stages of Swelling of Thin PNIPAM Films Using in Situ GISAXS Microfluidics. *Langmuir* **2015**, *31* (35), 9619−9627.
(50) Widmann, T.; Kreuzer, L. P.; Hohn, N.; Bießmann, L.; Wang, K.; Rinner, S.; Moulin, J.-F.; Schmid, A. J.; Hannappel, Y.; Wrede, O.; et al. Hydration and solvent exchange induced swelling and deswelling of homogeneous poly (*N*-isopropylacrylamide) microgel thin films. *Langmuir* **2019**, *35* (49), 16341−16352.
(51) Cubitt, R.; Fragneto, G. D17: the new reflectometer at the ILL. *Appl. Phys. A: Mater. Sci. Process.* **2002**, *74* (1), s329−s331.
(52) Müller-Buschbaum, P.; Cubitt, R.; Kosbahn, D.; Le Dû, M.; Reitenbach, J.; Spanier, L. *Investigation of the Influence of Salts on the Co-Nonsolvency Effect of Thin Polymer Films in Mixed Water/Dimethyl Sulfoxide Vapors*; Institut Laue-Langevin (ILL), 2023 .
(53) Sears, V. Neutron scattering lengths and cross-sections. *Neutron News* **1992**, *3*, 26−37.
(54) Sun, B.; Lin, Y.; Wu, P. Structure Analysis of Poly(N-isopropylacrylamide) Using Near-Infrared Spectroscopy and Generalized Two-Dimensional Correlation Infrared Spectroscopy. *Appl. Spectrosc.* **2007**, *61* (7), 765−771.
(55) Sun, B.; Lin, Y.; Wu, P.; Siesler, H. W. A FTIR and 2D-IR Spectroscopic Study on the Microdynamics Phase Separation Mechanism of the Poly(N-isopropylacrylamide) Aqueous Solution. *Macromolecules* **2008**, *41* (4), 1512−1520.
(56) Kyrey, T.; Witte, J.; Lutzki, J.; Zamponi, M.; Wellert, S.; Holderer, O. Mobility of bound water in PNIPAM microgels. *Phys. Chem. Chem. Phys.* **2021**, *23* (26), 14252−14259.
(57) Moreno, R. O.; Penott-Chang, E. K.; Rojas de Gáscue, B.; Müller, A. J. The effect of the solvent employed in the synthesis of hydrogels of poly (acrylamide-co-methyl methacrylate) on their structure, properties and possible biomedical applications. *Eur. Polym. J.* **2017**, *88*, 148−160.
(58) Vieira, J. N.; Posada, J. J.; Rezende, R. A.; Sabino, M. A. Starch and chitosan oligosaccharides as interpenetrating phases in poly(N-isopropylacrylamide) injectable gels. *Mater. Sci. Eng.* **2014**, *37*, 20−27.
(59) Dybal, J.; Trchová, M.; Schmidt, P. The role of water in structural changes of poly(N-isopropylacrylamide) and poly(N-isopropylmethacrylamide) studied by FTIR, Raman spectroscopy and quantum chemical calculations. *Vib. Spectrosc.* **2009**, *51* (1), 44−51.
(60) Liu, M.; Bian, F.; Sheng, F. FTIR study on molecular structure of poly(N-isopropylacrylamide) in mixed solvent of methanol and water. *Eur. Polym. J.* **2005**, *41* (2), 283−291.
(61) Custodio, K. K. S.; Claudio, G. C.; Nellas, R. B. Structural Dynamics of Neighboring Water Molecules of N-Isopropylacrylamide Pentamer. *ACS Omega* **2020**, *5* (3), 1408−1413.
(62) Franks, F.; Eagland, D.; Lumry, R. The Role of Solvent Interactions in Protein Conformatio. *CRC Crit. Rev. Biochem.* **1975**, *3* (2), 165−219.
(63) Ahmed, Z.; Gooding, E. A.; Pimenov, K. V.; Wang, L.; Asher, S. A. UV resonance Raman determination of molecular mechanism of poly (N-isopropylacrylamide) volume phase transition. *J. Phys. Chem. B* **2009**, *113* (13), 4248−4256.
(64) Pang, X.; Wang, K.; Cui, S. Single-chain mechanics of poly(N-isopropyl-acrylamide) in the water/methanol mixed solvent. *Polymer* **2013**, *54* (14), 3737−3743.
(65) Galbraith, M. L.; Madura, J. D. Identifying trends in hydration behavior for modifications to the hydrophobicity of poly(n-isopropylacrylamide). *J. Mol. Graphics Modell.* **2017**, *78*, 168−175.
(66) Harms, S.; Rätzke, K.; Faupel, F.; Egger, W.; Ravello, L.; Laschewsky, A.; Wang, W.; Müller-Buschbaum, P. Free Volume and Swelling in Thin Films of Poly(*N*-isopropylacrylamide) End-Capped with n-Butyltrithiocarbonate. *Macromol. Rapid Commun.* **2010**, *31* (15), 1364−1367.
(67) Mukherjee, M.; Souheib Chebil, M.; Delorme, N.; Gibaud, A. Power law in swelling of ultra-thin polymer films. *Polymer* **2013**, *54* (17), 4669−4674.
(68) Van Durme, K.; Van Assche, G.; Van Mele, B. Kinetics of demixing and remixing in poly (*N*-isopropylacrylamide)/water studied by modulated temperature DSC. *Macromolecules* **2004**, *37* (25), 9596−9605.
(69) Li, J.-J.; Zhou, Y.-N.; Luo, Z.-H. Thermal-responsive block copolymers for surface with reversible switchable wettability. *Ind. Eng. Chem. Res.* **2014**, *53* (47), 18112−18120.
(70) Nuopponen, M.; Kalliomäki, K.; Laukkanen, A.; Hietala, S.; Tenhu, H. A−B−A stereoblock copolymers of N-isopropylacrylamide. *J. Polym. Sci., Part A: Polym. Chem.* **2008**, *46* (1), 38−46.
(71) Biswas, C. S.; Patel, V. K.; Vishwakarma, N. K.; Tiwari, V. K.; Maiti, B.; Maiti, P.; Kamigaito, M.; Okamoto, Y.; Ray, B. Effects of tacticity and molecular weight of poly (N-isopropylacrylamide) on its glass transition temperature. *Macromolecules* **2011**, *44* (14), 5822−5824.

https://doi.org/10.1021/acs.macromol.4c02802
Macromolecules 2025, 58, 1000−1010